



Anomalous Depletion of Pore-Confined Carbon Dioxide upon Cooling below the Bulk Triple Point: An *In Situ* Neutron Diffraction Study

K. L. Stefanopoulos,¹ F. K. Katsaros,¹ Th. A. Steriotis,^{1,*} A. A. Sapalidis,¹ M. Thommes,²
D. T. Bowron,³ and T. G. A. Youngs³

¹*Institute of Nanoscience and Nanotechnology, NCSR “Demokritos”, 15310 Ag. Paraskevi Attikis, Athens, Greece*

²*Quantachrome Instruments, 1900 Corporate Drive, Boynton Beach, Florida, USA*

³*ISIS Neutron and Muon Source, STFC Rutherford Appleton Laboratory, Harwell Oxford, Didcot OX11 0QX, United Kingdom*

(Received 9 July 2015; published 14 January 2016)

The phase behavior of sorbed CO₂ in an ordered mesoporous silica sample (SBA-15) was studied by neutron diffraction. Surprisingly, upon cooling our sample below the bulk critical point, confined CO₂ molecules neither freeze nor remain liquid as expected, but escape from the pores. The phenomenon has additionally been confirmed gravimetrically. The process is reversible and during heating CO₂ refills the pores, albeit with hysteresis. This depletion was for the first time observed in an ordered mesoporous molecular sieve and provides new insight on the phase behavior of nanoconfined fluids.

DOI: 10.1103/PhysRevLett.116.025502

Fluids in confined environments are relevant in diverse areas spanning gas storage and separations, catalysis, oil extraction, and geological water management through to the engineering of microfluidic devices. Especially in nanoscale pores, the combination of solid-fluid interactions and finite volume can alter the structural and dynamic properties of fluids and strongly influence their phase behavior [1–4]. Although pore condensation has been thoroughly studied, mainly with the aid of ordered mesoporous materials, the freezing of fluids sorbed in nanopores is an intense field of research and a comprehensive theory on the phase behavior of pore-confined fluids is yet to be established. Among several cases, the freezing of water in ordered mesoporous silicas has been extensively studied [5–10]. The results suggest that water crystallizes in the core of the pores, at a temperature below the bulk freezing point according to the Gibbs-Thomson (GT) equation [8]. In contrast, surface-adsorbed water has liquid-like properties, while water confined in micropores cannot crystallize even at temperatures as low as 173 K [11]. CO₂ is another interesting candidate to study confinement effects because of its linear shape and quadrupole moment (both producing orientational correlations). Although bulk CO₂ has been thoroughly investigated, only limited experiments concerning confinement in nanoporous materials have been reported. It has generally been shown that above the bulk triple point, T_3 , and even at supercritical conditions, adsorbed CO₂ has a liquidlike structure in the pores while stronger orientational correlations have been observed [12–15]. On the other hand, confined CO₂ below its bulk triple point ($T_3 = 216.6$ K) is seldom investigated; for instance, so far, phase transitions that may occur below T_3 have not been studied in ordered mesopores. An x-ray diffraction (XRD) study of solidified CO₂ in a Vycor porous glass (mean pore diameter 70 Å) revealed a solid

with identical structure but decreased density compared to bulk CO₂, while the crystallite size was surprisingly larger (160 Å) than the pore size [16]. Further, positron annihilation experiments of sorbed CO₂ showed a depression of the triple point inside the pores of Vycor glass and an unexplained complex phase behavior at reduced CO₂ pressures [17]. Overall, the structure and properties of pore-confined CO₂ below T_3 remains largely unknown, and thus we attempt, for the first time, to monitor its phase behavior in the well-defined pores of the ordered mesoporous silica SBA-15 below 216 K by *in situ* neutron diffraction.

The experiments were carried out at the Near and Intermediate Range Order Diffractometer (NIMROD, ISIS Neutron Source, STFC Rutherford Appleton Laboratory, UK). The instrument delivers high neutron flux, moderate Q resolution, high detector stability, and low scattering backgrounds [18,19]. NIMROD bridges the gap between conventional small- and wide-angle neutron scattering and is thus ideally suited for *in situ* sorption experiments with ordered mesoporous materials. By conducting such experiments the evolution of the strong SANS diffraction signal of the porous structure (giving unique information on the spatial distribution of the adsorbed phase) can be monitored simultaneously with wide-angle data that highlight the molecular structure of the confined phase. For the *in situ* measurements a special adsorption apparatus has been constructed [14,20]. Approximately 0.85 g of outgassed (12 h, 500 K, 10⁻⁶ mbar) SBA-15 powder silica (Claytec Inc.), were placed into a null scattering Ti_{0.676}Zr_{0.324} cell. Measurements of bulk liquid and bulk solid CO₂ were also carried out. The scattered neutrons were counted as a function of neutron time-of-flight, corrected for instrument and container backgrounds, absorption and multiple scattering, and normalized to a

standard vanadium scatterer using Gudrun analysis routines [21,22].

Figure 1 (inset) illustrates the CO₂ isotherm of SBA-15 at 214 K (i.e., slightly below T_3) measured gravimetrically (IGA, HidenIsochema). As in the case of N₂ at 77 K [23], the isotherm is typical for a mesoporous material with cylindrical pores of uniform size (type IV, H1 hysteresis loop). Figure 1 also shows the *in situ* neutron measurements that were carried out (outgassed sample, just before and after the capillary condensation region). The small-angle diffraction pattern of dry SBA-15 exhibits three Bragg peaks, namely, (10), (11), and (20), due to the regular 2D hexagonal packing of mesopores [27]. Additionally, the amorphous “glasslike” structure of the SBA-15 silica walls is visible at high Q . On the other hand, the small-angle profile of partially filled SBA-15 at 3.3 bar of CO₂ differs remarkably; the (10) and (20) intensities increase, (11) becomes very weak while two additional reflections, (21) and (30), appear. The above can be explained after considering the structure of SBA-15 and the adsorption process. SBA-15 has 2D ordered mesopores while disordered micropores are found in the pore walls. Moreover, a less dense SiO₂ corona is located on the surface of the ordered mesopores. At the initial stages of adsorption micropores are filled; as the pressure increases layers of adsorbed CO₂ that cover the corona are formed. Thus, just before capillary condensation (3.3. bar) both the pore walls and the corona appear more dense (due to the extra adsorbed CO₂). In this respect, the contrast between the walls and the empty ordered mesopores increases substantially (main peak intensity increase), while the long-range order of the pore lattice is fully resolved (appearance of new peaks) [14,29]. Furthermore, at

3.3 bar, the main peak of confined CO₂ ($Q \sim 1.8 \text{ \AA}^{-1}$) is clearly visible at high Q . At $P = 3.8$ bar, capillary condensation is complete and the pores are filled with condensate (filled SBA-15). The scattering profile of the filled sample has the same features, with the empty case exhibiting again only three reflections. However, due to lower contrast (SiO₂-CO₂ compared to SiO₂ vacuum) the peak intensity is decreased by almost 1 order of magnitude. On the other hand, the intensity of the confined CO₂ peak is further increased, as expected. In the very low Q regime ($Q < 0.04 \text{ \AA}^{-1}$), an enhanced signal is observed for both adsorption stages. This can be explained as after adsorption the SBA-15 grains have a higher scattering length density (due to the adsorbed CO₂) and thus the contrast between the practically empty intergrain space and the grains increases giving rise to a stronger SANS signal. The total-scattering structure factors and differential correlation functions of bulk (liquid and solid) and confined CO₂ have been deduced and compared. The confined CO₂ has liquidlike properties although subtle differences are observed, pointing to stronger orientational correlations, especially at the stage before capillary condensation. These differences were attributed to either pore wall-fluid interactions (adsorbed film) or the confinement of the fluid (when pores are filled), combined with the relatively large quadrupole moment of CO₂ [30]. Finally, the pore-confined CO₂ density of the filled sample has been calculated from the integrated intensity of the main Bragg reflection ($d = 1.10 \text{ g/cm}^3$, i.e., very close to the 1.18 g/cm^3 density of the bulk liquid) [36].

As a next step, SBA-15 was slightly heated above T_3 for avoiding external dry ice formation. Then it was further filled with successive loadings of CO₂ (up to $P = 5.18$ bar) to ascertain that all pores as well as the measuring cell were completely filled with liquid CO₂. The cell was then subject to slow cooling down to 212 K (0.3 K/min). During the cooling process at about 214 K a “transient” spectrum was recorded. In this case (overfilled SBA-15), only the (10), (11), and (20) peaks are visible, as in the case of the filled sample, and the SANS intensity is further reduced (since the intergrain space is also filled). In addition, a very strong peak from liquid CO₂ (at $Q \sim 1.8 \text{ \AA}^{-1}$) is evident. Again, from the reduced integrated intensity of the (10) peak the calculated density of the pore carbon dioxide is increased to $d = 1.29 \text{ g/cm}^3$ [36]. This causes lowering of contrast, resulting in a weaker and correspondingly more noisy “jagged” low- Q signal. The next pattern at 212 K shows clearly the Bragg reflections from solid CO₂ [see also Fig. 2(a), inset]. The peaks are identical to those obtained from bulk dry ice without any noticeable broadening [41]. This implies that only external CO₂ between silica particles is solidified. Moreover, if solidification occurs also within the pore matrix one should expect a significant decrease of the SANS signal and probably the elimination of the Bragg peaks because the scattering length

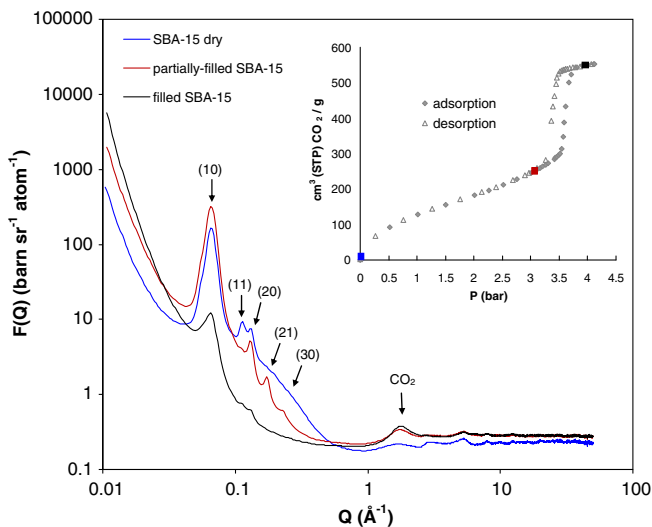


FIG. 1. Diffraction patterns of SBA-15 during CO₂ adsorption at 214 K. Inset: CO₂ adsorption isotherm at 214 K; the square symbols show the points where *in situ* neutron diffraction measurements were performed.

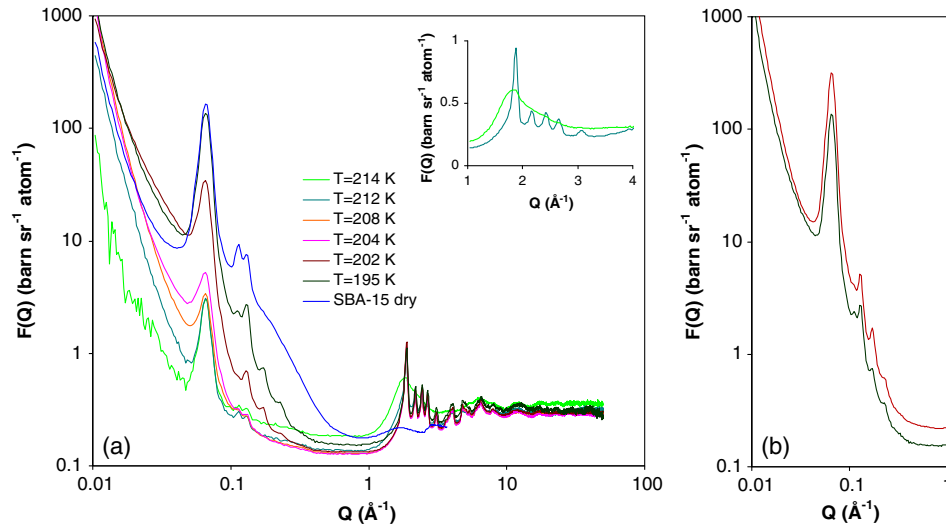


FIG. 2. (a) Diffraction profiles of SBA-15 overfilled with CO_2 ($T = 214$ K) during the freezing process. The pattern of dry SBA-15 is also presented for comparison. Inset: Highlight of the liquid-solid transition of the external CO_2 ; (b) SANS curves of partially filled SBA-15 at 214 K (red) and SBA-15 during freezing at 195 K (green).

density (SLD) of silica almost “matches” that of dry ice, resulting in an almost perfect contrast matching. In contrast to this hypothesis, the intensity of the (10) reflection is practically the same, suggesting that the density of pore-confined CO_2 remains almost unaltered [36]. The remarkable increase of the low- Q intergrain scattering signal is due to enhanced contrast arising from the liquid carbon-dioxide filled SiO_2 particles and the external dry ice [45].

As freezing progresses, one would expect solidification of CO_2 confined in the pore network according to the GT equation. This was actually observed by differential scanning calorimetry (DSC) measurements for confined water in a series of SBA-15 samples; when external water was present (overfilled pores), freezing occurred at a temperature that almost obeyed the GT equation [46]. Again, in a recent study [5], DSC and XRD measurements carried out in SBA-15 samples overfilled with water revealed initial crystallization of external water followed by the freezing of

confined pore water at a temperature depending on the pore size. In our case, the relatively large pore size (74 \AA) would imply a rather small depression of the freezing point. However, as mentioned, if confined CO_2 solidifies in the pores, a significant drop of the SANS signal is expected due to contrast matching. Surprisingly, upon freezing, a gradual increase of the SANS intensity is observed followed by the appearance of the (21), (30) peaks [Fig. 2(a)]. When the temperature reaches 195 K the SANS curve becomes similar with that of the partially filled sample [Fig. 2(b)]. These unexpected results provide strong evidence that upon cooling, CO_2 molecules instead of crystallizing, escape from the pores and only the adsorbed film remains. The intensity increase of the main Bragg peak suggests that depletion commences at about 208 K.

Figure 3(a) shows that upon heating the process is reversible, however, with a temperature hysteresis. In brief, upon heating, CO_2 progressively reenters the pores and

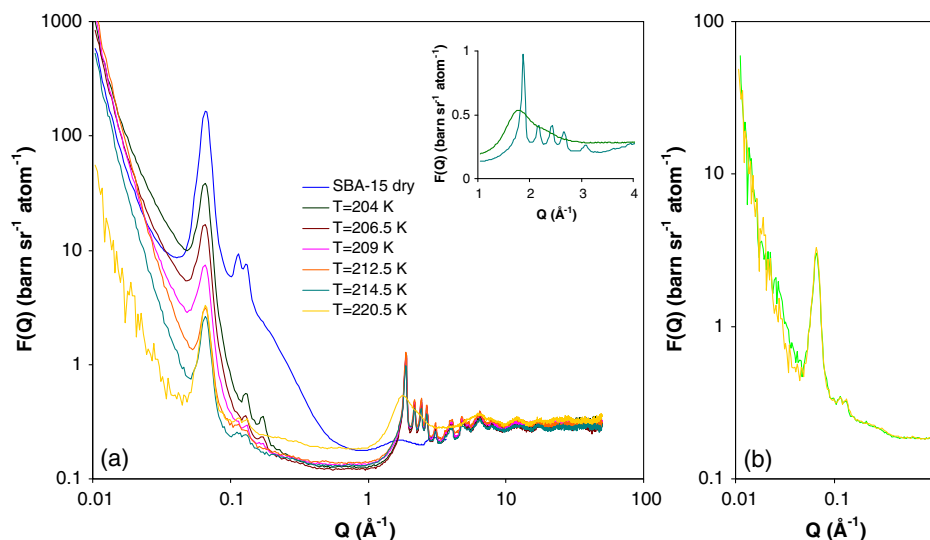


FIG. 3. (a) Diffraction profiles of SBA-15 during heating. The pattern of dry SBA-15 is also presented for comparison. Inset: Highlight of the solid-liquid transition of external CO_2 . (b) SANS curves of overfilled SBA-15 at 214 K (green) and SBA-15 during heating at 220.5 K (yellow).

condensation takes place [Fig. 3(a), inset] since the SANS intensity reduces and a strong diffraction peak of liquid CO₂ finally emerges, revealing that all pores are overfilled, with the presence of external liquid CO₂. It is noteworthy that the SANS curve at 220.5 K is identical with that at 214 K (overfilled sample) suggesting that the process is fully reversible, associated with a temperature hysteresis [Fig. 3(b)].

This peculiar depletion phenomenon has been further confirmed by independent gravimetric measurements as described in the Supplemental Material [47]. The gravimetric data revealed that during freezing in the CO₂ loaded SBA-15 sample below T_3 , depletion takes place at around 208 K (monitored by significant weight loss) and only the adsorbed film remains. Upon heating, condensation occurs, and results in pore filling. The results are in excellent agreement with the neutron measurements.

A similar “depletion” behavior has only been observed once by means of torsional oscillator measurements during freezing of partially hydrogen filled porous Vycor glass below the triple point of bulk H₂ [48]. However, in contrast to our results, when the sample was completely filled, solidification occurred within the pore system, while new studies have confirmed that H₂ solidifies within the pores of several materials, including Vycor glass [4,49]. Further, positron or positronium annihilation spectroscopy studies for the CO₂-Vycor system implied a drastic signal change below T_3 . The unexpected signal increase was explained in terms of creation of empty space within the pores [50]; however, it might also be compatible with CO₂ depletion. It should be stressed that while these previous observations were made in Vycor (a highly disordered silica material with an ill-defined pore network), our study proves the existence of a depletion phenomenon in a highly ordered mesoporous silica molecular sieve (SBA-15) which exhibits a narrow distribution of cylindrical pores.

Such a spontaneous depletion can initially be explained by simply considering that during cooling the vapor pressure of the bulk phase (solid CO₂) drops below the relative pressure where desorption of the supercooled condensate should occur. Thus, in a simplistic fashion, depletion occurs because the “external” pressure is too low. Of course, the depletion has deeper implications as it is directly connected with the pore size of the adsorbent and its ability to maintain a stable pore condensate. In terms of thermodynamics, since there is a certain temperature (208 K in our case) where molecules “prefer” to escape and solidify in the bulk rather than remain sorbed in the pores, one could conclude that for our system (SBA-15) this is a characteristic temperature where the free energy of the pore condensate is higher than the free energy of the bulk solid CO₂. It should, however, be clearly pointed out that the particular experimental conditions as well as the

thermodynamic properties of CO₂ gave us a unique “working window” to observe this new phenomenon. In detail, in our neutron scattering experiment the “external” volume of the cell allowed enough space to accommodate the depleted CO₂ molecules (this space was obviously created because of the volume contraction of the solid upon cooling). Likewise, our gravimetric experiment was designed in such a way that bulk solid CO₂ could be formed only on the walls of our reactor while the sample was always in equilibrium with vapors (the vapor pressure of the solid CO₂). In both cases (gravimetry and neutrons) the system was not connected to an external CO₂ vapor source (in the neutron cell because of CO₂ solidification that effectively blocked the vapor access to the sample and in gravimetry because we used an isolation valve). In this respect we may state our findings more accurately. For our system (SBA-15/CO₂) there exists no “pore triple point” (gas-liquid-solid coexistence) when pores are in contact with the bulk phase (gas-solid below T_3). However, there is a characteristic temperature (208 K) below which the condensed CO₂ phase destabilizes, escapes from the pores and solidifies as bulk. Finally, it should be pointed out that simulation studies in “isolated” pores (such as GCMC for instance) would not be able to predict this phenomenon because they do not take into account the interaction with the bulk phase.

In conclusion, neutron diffraction and gravimetric measurements revealed that during freezing below the bulk triple point, pore condensed CO₂ molecules, instead of crystallizing, escape from the pores of SBA-15 and only the adsorbed film remains; solidification occurs only in the external region between the silica particles. Finally, the results show that upon heating the process is fully reversible, associated, however, with a temperature hysteresis between depletion and condensation.

The thermodynamics of confined nanophases is an intense field of research [51]. Our experimental findings highlight previously unknown details of the phase behavior of pore-confined fluids and as such may help in developing a thermodynamically consistent holistic theory. We expect that the interplay between pore size and attractive adsorbate-adsorbent interactions, as well as of the properties of the bulk phase, should play a major role in determining whether and how the described depletion phenomenon may occur (e.g., for different pore sizes, other gases, etc.). More experimental and simulation work is thus necessary to understand the underlying mechanism of the observed depletion phenomenon. Such systematic studies utilizing mesoporous molecular sieves with different pore sizes and pore geometries are currently underway.

This project has received funding from the European Union’s 7th Framework Programme for research, technological development and demonstration under the NMI3-II Grant No. 283883.

- *.steriotis@inn.demokritos.gr
- [1] C. Alba-Simionesco, B. Coasne, G. Dosseh, G. Dudziak, K. E. Gubbins, R. Radhakrishnan, and M. Sliwinska-Bartkowiak, *J. Phys. Condens. Matter* **18**, R15 (2006).
- [2] H. K. Christenson, *J. Phys. Condens. Matter* **13**, R95 (2001).
- [3] L. D. Gelb, K. E. Gubbins, R. Radhakrishnan, and M. Sliwinska-Bartkowiak, *Rep. Prog. Phys.* **62**, 1573 (1999).
- [4] T. Hofmann, P. Kumar, M. Enderle, and D. Wallacher, *Phys. Rev. Lett.* **110**, 065505 (2013).
- [5] S. Kittaka, Y. Ueda, F. Fujisaki, T. Iiyama, and T. Yamaguchi, *Phys. Chem. Chem. Phys.* **13**, 17222 (2011).
- [6] J. Seyed-Yazdi, J. C. Dore, J. Beau W. Webber, and H. Farman, *J. Phys. Condens. Matter* **25**, 465105 (2013); J. Seyed-Yazdi, H. Farman, J. C. Dore, J. Beau W. Webber, G. H. Findenegg, and T. Hansen, *J. Phys. Condens. Matter* **20**, 205107 (2008).
- [7] M. Sliwinska-Bartkowiak, M. Jazdzewska, L. L. Huang, and K. E. Gubbins, *Phys. Chem. Chem. Phys.* **10**, 4909 (2008).
- [8] G. H. Findenegg, S. Jähnert, D. Akcakayiran, and A. Schreiber, *ChemPhysChem* **9**, 2651 (2008).
- [9] K. Morishige and H. H. Iwasaki, *Langmuir* **19**, 2808 (2003).
- [10] R. Schmidt, E. W. Hansen, M. Stöcker, D. Akporiaye, and O. H. Ellestad, *J. Am. Chem. Soc.* **117**, 4049 (1995).
- [11] F. G. Alabarse, J. Haines, O. Cambon, C. Levelut, D. Bourgogne, A. Haidoux, D. Granier, and B. Coasne, *Phys. Rev. Lett.* **109**, 035701 (2012).
- [12] Y. B. Melnichenko, G. D. Wignall, D. R. Cole, and H. Frielinghaus, *J. Chem. Phys.* **124**, 204711 (2006).
- [13] T. A. Steriotis, K. L. Stefanopoulos, N. K. Kanellopoulos, A. C. Mitropoulos, and A. Hoser, *Colloids Surf. A* **241**, 239 (2004).
- [14] T. A. Steriotis, K. L. Stefanopoulos, F. K. Katsaros, R. Gläser, A. C. Hannon, and J. D. F. Ramsay, *Phys. Rev. B* **78**, 115424 (2008).
- [15] K. L. Stefanopoulos, T. A. Steriotis, F. K. Katsaros, N. K. Kanellopoulos, A. C. Hannon, and J. D. F. Ramsay, *J. Phys. Conf. Ser.* **340**, 012049 (2012).
- [16] D. W. Brown, P. E. Sokol, A. P. Clarke, M. A. Alam, and W. J. Nuttall, *J. Phys. Condens. Matter* **9**, 7317 (1997).
- [17] H. M. Fretwell, J. A. Duffy, A. P. Clarke, M. A. Alam, and R. Evans, *J. Phys. Condens. Matter* **8**, 9613 (1996).
- [18] D. T. Bowron and A. K. Soper, *Neutron News* **22**, 12 (2011).
- [19] D. T. Bowron, A. K. Soper, K. Jones, S. Ansell, S. Birch, J. Norris, L. Perrott, D. Riedel, N. J. Rhodes, S. R. Wakefield, A. Botti, M.-A. Ricci, F. Grazzi, and M. Zoppi, *Rev. Sci. Instrum.* **81**, 033905 (2010).
- [20] See Supplemental Material at <http://link.aps.org/supplemental/10.1103/PhysRevLett.116.025502>, Sec. 1, which includes Ref. [14], for more experimental details.
- [21] P. Day, J. E. Enderby, W. G. Williams, L. C. Chapon, A. C. Hannon, P. G. Radaelli, and A. K. Soper, *Neutron News* **15**, 19 (2004).
- [22] A. C. Hannon, W. S. Howells, and A. C. Soper, in *Neutron Scattering Data Analysis 1990*, edited by M. W. Johnson, IOP Conf. Proc. No. 107 (IOP, Bristol, 1990), p. 193.
- [23] See Supplemental Material at <http://link.aps.org/supplemental/10.1103/PhysRevLett.116.025502>, Sec. 2.1, which includes Refs. [24–26], for the structural parameters of SBA-15 obtained by the N₂ isotherm.
- [24] K. S. W. Sing, D. H. Everett, R. A. W. Haul, L. Moscou, R. A. Pierotti, J. Rouquérol, and T. Siemieniewska, *Pure Appl. Chem.* **57**, 603 (1985).
- [25] E. P. Barret, L. G. Joyner, and P. H. Halenda, *J. Am. Chem. Soc.* **73**, 373 (1951).
- [26] A. V. Neimark, *Langmuir* **11**, 4183 (1995); P. I. Ravikovitch, S. C. O. Domhnaill, A. V. Neimark, F. Schueth, and K. K. Unger, *Langmuir* **11**, 4765 (1995).
- [27] See Supplemental Material at <http://link.aps.org/supplemental/10.1103/PhysRevLett.116.025502>, Sec. 2.2, which includes Ref. [28], for the deduced differential cross section and the pair correlation function of SBA-15.
- [28] S. Kallus, A. Hahn, and J. D. F. Ramsay, *Eur. Phys. J. E* **12**, S31 (2003).
- [29] D. Mütter, S. Jähnert, J. W. C. Dunlop, G. H. Findenegg, and O. Paris, *J. Phys. Chem. C* **113**, 15211 (2009).
- [30] See Supplemental Material at <http://link.aps.org/supplemental/10.1103/PhysRevLett.116.025502>, Secs. 3.1 and 4.1, which include Refs. [14–15,31–35], for the structural characteristics of bulk liquid and confined CO₂, respectively. The liquidlike properties of confined carbon dioxide have also been observed in MCM-41 during adsorption at 253 K; see for details, Ref. [14].
- [31] A. K. Adya and C. J. Wormald, *Mol. Phys.* **74**, 735 (1991).
- [32] J. B. van Tricht, H. Fredrikze, and J. van der Laan, *Mol. Phys.* **52**, 115 (1984).
- [33] S. Chiappini, M. Nardone, and F. P. Ricci, *Mol. Phys.* **89**, 975 (1996).
- [34] De Santis, R. Frattini, D. Gazzillo, and M. Sampoli, *Mol. Phys.* **60**, 21 (1987).
- [35] C. Alba-Simionesco, G. Dosseh, E. Dumont, B. Frick, B. Geil, D. Morineau, V. Teboul, and Y. Xia, *Eur. Phys. J. E* **12**, 19 (2003).
- [36] See Supplemental Material at <http://link.aps.org/supplemental/10.1103/PhysRevLett.116.025502>, Sec. 4.2, which includes Refs. [14,37–40], for the density calculations.
- [37] D. Morineau, R. Guégan, Y. Xia, and C. Alba-Simionesco, *J. Chem. Phys.* **117**, 8966 (2002).
- [38] M. Erko, D. Wallacher, A. Brandt, and O. Paris, *J. Appl. Crystallogr.* **43**, 1 (2010).
- [39] T. Shin, G. H. Findenegg, and A. Brandt, *Prog. Colloid Polym. Sci.* **133**, 116 (2006).
- [40] Asia Industrial Gases Association, CARBON DIOXIDE AIGA 068/10 Globally Harmonized Document Based on CGA G-6, 7th Edition, (Asia Industrial Gases Association, Singapore, 2009), p. 35.
- [41] See Supplemental Material at <http://link.aps.org/supplemental/10.1103/PhysRevLett.116.025502>, Sec. 3.2, which includes Refs. [42–44], for the diffraction pattern of bulk dry ice. For the broadening of the main Bragg reflection observed in crystalline benzene confined in SBA-15, see also Ref. [1], Fig. 5.
- [42] C. S. Yoo, H. Cynn, F. Gygi, G. Galli, V. Iota, M. Nicol, S. Carlson, D. Häusermann, and C. Mailhot, *Phys. Rev. Lett.* **83**, 5527 (1999).
- [43] W. H. Keesom and J. W. L. Köhler, *Physica (Amsterdam)* **1**, 167 (1934).

- [44] A. Simon and K. Peters, *Acta Crystallogr. Sect. B* **36**, 2750 (1980).
- [45] See Supplemental Material at <http://link.aps.org/supplemental/10.1103/PhysRevLett.116.025502>, Sec. 5, for the discussion of the intergrain scattering.
- [46] A. Schreiber, I. Ketelsen, and G. H. Findenegg, *Phys. Chem. Chem. Phys.* **3**, 1185 (2001).
- [47] See Supplemental Material at <http://link.aps.org/supplemental/10.1103/PhysRevLett.116.025502>, Sec. 6, for the gravimetric experiment.
- [48] M. Schindler, A. Dertinger, Y. Kondo, and F. Pobell, *Phys. Rev. B* **53**, 11451 (1996).
- [49] E. Van Cleve, M. A. Worsley, and S. O. Kucheyev, *J. Appl. Phys.* **116**, 163517 (2014); S. O. Kucheyev, E. Van Cleve, and M. A. Worsley, *J. Phys. Condens. Matter* **26**, 225004 (2014); Y. J. Glanville, J. V. Pearce, P. E. Sokol, B. Newalker, and S. Komarneni, *Chem. Phys.* **292**, 289 (2003); G. Beaudoin, P. Haljan, M. Paetkau, and J. R. Beamish, *J. Low Temp. Phys.* **105**, 113 (1996).
- [50] J. A. Duffy and M. A. Alam, *Langmuir* **16**, 9513 (2000).
- [51] K. E. Gubbins, Y. Long, and M. Śliwinska-Bartkowiak, *J. Chem. Thermodyn.* **74**, 169 (2014).